ACS OMEGA

Open Access

http://pubs.acs.org/journal/acsodf

Article

Anti-inflammatory Properties of Tongfeng Li'an Granules in an Acute Gouty Arthritis Rat Model

Xiangpei Zhao, Zhaoyang Long, Hua Zhong, Rongping Lu, Juan Wei, Fengzhen Li,*,† and Zongxi Sun*,†

Cite This: *ACS Omega* 2024, 9, 34303−34313

Read Online

ACCESS | Metrics & More | Article Recommendations

ABSTRACT: Objectives: To examine the anti-inflammatory properties and underlying mechanisms of Tongfeng Li'an Granules (TFLA), a traditional medicine, in acute gouty arthritis using a rat model. Materials and Methods: We identified 55 major compounds in TFLA via ultrahigh-performance liquid chromatography connected to quadrupole time-of-flight mass spectrometry (UPLC-TQF-MS/MS). Databases were employed for the prediction of potential targets, followed by PPI network construction as well as GO and KEGG analyses. After network-pharmacology-based analysis, a rat gouty arthritis model was used to validate the anti-inflammatory mechanism of TFLA. Results: UPLC-TQF-MS/MS and network pharmacology analyses revealed 55 active ingredients and 160 targets of TFLA associated with gouty arthritis, forming an ingredient-target-disease network. The PPI network identified 20 core targets, including TLR2, TLR4, IL6, NFκB, etc. Functional enrichment analyses highlighted the Toll-like receptor signaling pathway as significantly enriched by multiple targets, validated in in vivo experiments. Animal experiments demonstrated that TFLA improved pathological changes in gouty joint synovium, with decreased ankle joint circumference, serum IL6, IL10, and TNFα levels, as well as reduced protein and mRNA expression of NLRP3, TLR2, and TLR4 in ankle joint synovial tissue observed in the middle- and high-dose TFLA and positive control groups compared to the model group ($p < 0.05$). Conclusion: This research elucidated the pharmacological mechanisms of TFLA against gouty arthritis, implicating various ingredients, targets, and signaling pathways. Animal experiments confirmed TFLA's efficacy in alleviating inflammation in acute gouty arthritis by modulating Toll-like receptor signaling and NLRP3 expression.

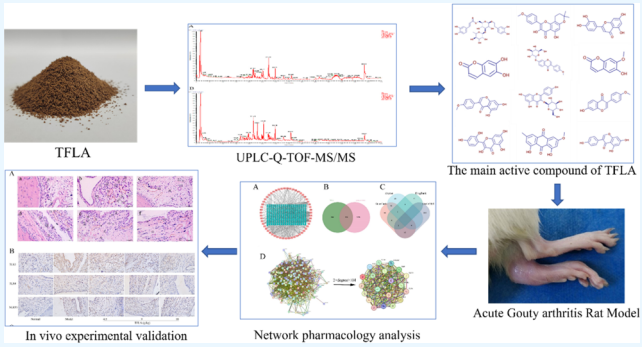

INTRODUCTION

Gout, a condition arising from disruptions in purine metabolism,[1] manifests as the deposition of monosodium urate (MSU) monohydrate crystals in bones, joints, kidneys, and subcutaneous tissue.[2] It is primarily driven by heightened uric acid synthesis, often compounded by acute and chronic inflammation and tissue damage.[3,4] The prevalence of gout has surged in recent decades, marking it as a prevalent form of inflammatory arthritis, particularly afflicting men.[5−8] Major risk factors for its onset include hyperuricemia, age, genetic predispositions, dietary patterns, alcohol intake, metabolic syndrome, hypertension, obesity, diuretic use, cholesterol levels, and chronic kidney disease.[9] Among the contemporary antigout drugs, colchicine remains a mainstay of treatment due to its efficacy in mitigating the frequency and severity of gout attacks by suppressing inflammatory pathways. However, its narrow therapeutic window and potential toxicity, especially in cases of overdose, raise considerable concerns. Common adverse effects include gastrointestinal upset, neutropenia, and neuromuscular toxicities. Allopurinol, which is an inhibitor of xanthine oxidase, is another commonly prescribed drug for gout management. It operates by lowering uric acid levels, thereby reducing the risk of gout flares. However, some patients may experience a hypersensitivity syndrome, necessitating cautious dosage adjustments and monitoring, while renal impairment can limit its applicability. Febuxostat, a newer alternative to allopurinol, also targets xanthine oxidase inhibition with enhanced potency, which is particularly beneficial for patients with renal impairments. Nevertheless, its elevated cost and limited long-term safety profile warrant careful consideration in clinical use.[10]

In contrast to synthetic drugs, natural products offer promising alternatives for managing gout. These encompass a wide range of herbs, dietary supplements, and phytomedicines known for their anti-inflammatory and antiarthritic properties.

Received: January 3, 2024
Revised: July 13, 2024
Accepted: July 22, 2024
Published: July 31, 2024

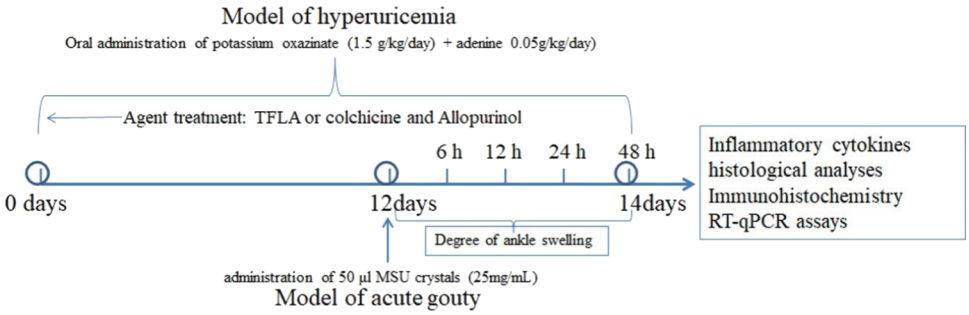

Figure 1. Experimental design.

Their benefits extend to a more holistic approach to health, fewer side effects, and potential cost-effectiveness.[11−13] However, while natural products present a complementary avenue with reduced side effects, their safety and efficacy require more investigations. Subsequent studies should concentrate on clarifying their underlying mechanisms, optimizing dosages, and evaluating long-term outcomes in the management of gouty arthritis.[14−16]

TFLA, composed of *Sarcandra glabra* (Thunb.) Nakai, *Dioscorea hypoglauca* Palibin, *Plantago asiatica* L., *Polygonum cuspidatum* Sieb.et Zucc., *Cynanchum paniculatum* (Bunge) Kitag., Speranskiatuberculata (Bunge) Baill., Lonicerachrysantha Turcz., and *Glycyrrhiza uralensis* Fisch, is a clinical empirical prescription originating from a Zhuang ethnic minority area in Southwest China, which has been in use for over 2 decades. TFLA has demonstrated significant efficacy in alleviating joint pain, swelling, and activity limitations in acute gout attacks while also showing promise in reducing uric acid and enhancing joint function in the chronic stage of gout, all without apparent adverse effects. However, despite its evident benefits, the precise mechanisms of action remain elusive. This research aims to investigate the anti-inflammatory effects and underlying mechanisms of TFLA in acute gouty arthritis using a rat model.

MATERIALS AND METHODS

Drugs and Reagents. TFLA was produced by the Pharmaceutical Factory of Guangxi University of Traditional Chinese Medicine. Monosodium urate (MSU) was supplied by Sigma-Aldrich. Potassium oxonate (PO), Allopurinol, and Adenine were acquired from Shanghai yuanye Bio-Technology (China). Colchicine (COL) was supplied by XiShuangBanNa BanNa Phytopharmaceutical (China). TNFα, IL6, and IL10 ELISA kits and NLRP3, TLR2, and TLR4 antibodies were bought from Bioswamp (China). PVDF membrane and ECL reagent kit were obtained from Millipore. BCA protein assay kit and diaminobenzidine (DAB) staining kit were acquired from Solarbio (China). Cytoplasmic and nuclear extraction reagent kit was supplied by Beyotime Biotech (China). The biochemical parameter determination reagent kits were procured from Nanjing Jiancheng Bioengineering (China).

UPLC-TQF-MS/MS Analysis. For UPLC-TQF-MS/MS experiments,[17] a Q-Exactive-Plus-Orbitrap-High-Resolution-Liquid-Mass-Spectrometer (Thermo-Fisher) was connected to a U3000-UltraHigh-Performance Liquid Chromatography (Thermo-Fisher). Data detection and processing were conducted using Compound Discover 3.2 software. Chromatographic separation was conducted using an ACQUITY-UPLC-HSS-T3-C18 column (100 × 2.1 mm^2, 1.8 μm) at 35 °C. The mobile phase contained 0.1% formic acid−water (A) and 0.1% formic acid-acetonitrile (B) at 0.30 mL/min. A linear-gradient program was employed (30% B at 0−10 min, 30−40% B at 10−25 min, 40−50% B at 25−30 min, 50−70% B at 30−40 min, 70−100% B at 40−45 min, 100% B at 45−60 min, 100−0% B at 60−60.5 min, and 0% B at 60.5−70 min). The sample injection volume was 10 μL.

The mass spectrometry data acquisition was conducted using the Q-Exactive-Orbitrap-high-resolution-mass-spectrometry platform. The detection mode employed was Full MS-ddMS^2, with separate scans conducted in both negative and positive ion modes across the m/z range of 100−1200. The settings for MS^1 resolution were configured to 70,000, while MS^2 resolution was set at 17,500. The ion source voltage was maintained at 3.2 kV, with the capillary and auxiliary gas heater temperatures of 320 and 350 °C, respectively. The flow rates for auxiliary gas and sheath gas were set to 15 and 40 L/min, respectively, with an AGC Target of 1e6 and a TopN value of 5. Collision energy for MS^2 scans was incrementally adjusted at 30, 40, and 50 nm using the stepped NCE.

Network Pharmacology. The potential targets were searched from TCMSP based on the identified main ingredients of TFLA as described in a previous study.[18] Utilizing "Gouty arthritis" as a key term, targets related to this condition were searched in GeneCards (https://www.genecards.org/) and OMIM (https://omim.org/). Data obtained from these databases were merged, eliminating any duplicates. UniProt (https://www.uniprot.org/) was employed to assign a gene to each predicted target protein, exclusively focusing on "*Homo sapiens*". Intersection targets were obtained by importing disease targets into Venny v2.1.0 (https://bioinfogp.cnb.csic.es/tools/venny/). A protein−protein interaction (PPI) network was established based on the interaction targets identified with STRING (https://www.string-db.org/). The obtained diagram was input into Cytoscape v3.8.2 for topological analysis using the network analyzer. Core targets were chosen based on the card values of 2-fold degree medians, betweenness medians, and closeness medians. The resulting core targets were then analyzed using DAVID (https://david.ncifcrf.gov/), focusing solely on the "human" species, followed by KEGG analysis. An advanced bubble chart was utilized to visually represent the top 20 pathways based on their p-values.

Animals. Sixty Sprague−Dawley rats (age = 6−8 weeks, weight = 180−220 g) were sourced from Hunan SJA Laboratory Animal (China). The rats were maintained in controlled conditions (22 ± 1 °C, 50 ± 1% relative humidity, and a 12/12-h light/dark cycle). They were provided with unlimited access to water and food for 1 week. Ethical approval for the use of animals was granted from the Institutional Review Board of Guangxi University of Chinese Medicine (Approval No. DW2020618-31).

https://doi.org/10.1021/acsomega.4c00056
ACS Omega 2024, 9, 34303−34313

Table 1. Primer Sequence for Real-Time RT-PCR

target gene		sequence
NF-κB	forward primer	5′-GCAAACCTGGGAATACTTCATGTGACTAAG-3′
	reverse primer	5′-ATAGGCAAGGTCAGAATGCACCAGAAGTCC-3′
TLR2	forward primer	5′-GTACGCAGTGAGTGGTGCAAGT-3′
	reverse primer	5′-GGCCGCGTCATTGTTCTC-3′
TLR4	forward primer	5′-AATCCCTGCATAGAGGTACTTCCTAAT-3′
	reverse primer	5′-CTCAGATCTAGGTTCTTGGTTGAATAAG-3′
GADPH	forward primer	5′-AGTGCCAGCCTCGTCTCATA-3′
	reverse primer	5′-ACCAGCTTCCCATTCTCAGC-3′

Rat Gout Arthritis Model and Grouping. Fifty rats were randomly assigned to a positive group, model group, normal group, and TFLA-low, middle, and high-dose groups (n = 10/group). The rats in TFLA-low, middle, and high dose groups received 4.5, 9, and 18 g/kg/day TFLA granules, respectively. The positive group was given allopurinol (27 mg/kg/day) + colchicine (0.27 mg/kg/day), and the blank and model groups were given 10 mL/kg of pure water. Each group was given intragastric administration continuously for 14 days. Except for the blank group, which was given pure water, the other groups received adenine (0.05 g/kg) + potassium oxazinate (1.5 g/kg) solution by intragastric administration at 8 h after treatment. On the 12th day, 50 μL MSU crystals (25 mg/kg) were injected into the left ankle joint of rats for inducing acute gouty arthritis. The experimental design is shown in Figure 1.

Degree of Ankle Swelling. After injecting MSU crystals at intervals of 0, 6, 12, 24, and 48 h, the perimeter of the identical region of the ankle joint on the left hind limb of the rat was assessed using the ligature method. Subsequently, the swelling rate was calculated:[19,20] Swelling rate (%, n h) = (perimeter n h − perimeter 0 h)/perimeter of 0 h × 100%.

Inflammatory Cytokines Assays. Blood specimens were withdrawn from the abdominal aorta of rats prior to euthanasia. The samples were allowed to stand at 4 °C for 1 h and subsequently centrifuged at 3000 rpm for 15 min to isolate the serum. The separated serum specimens were then utilized to analyze the levels of IL6, IL10, and TNFα using kits procured from Bioswamp.[21]

Histological Observations. The left ankle joint was immobilized using a 4% paraformaldehyde solution, followed by decalcification with a 20% ethylenediamine tetraacetic acid solution. Subsequently, the tissue underwent dehydration through an ethanol gradient followed by embedding in paraffin. The embedded tissue was then sectioned, followed by HE staining. The resulting sections were examined under a microscope to assess inflammatory cell infiltration, edema, synovial hyperplasia, and vascular congestion within the synovial tissue.[22,23]

Immunohistochemistry. Immunohistochemical staining was conducted using the SABC method. Primary antibodies against TLR2, TLR4, and NLRP3 were employed accordingly, with all subsequent procedures performed according to the instructions provided with the kit. The new DAB substrate was utilized for color development, and the stain intensity was monitored by using a microscope. As a negative control, PBS was used in place of the primary antibody. Finally, 5 random fields of view were chosen from each section. The area of interest (AOI) and integrated optical density (IOD) were quantified using Image-Pro-Plus version 6.0, and the mean IOD/AOI ratio was determined to assess the extent of regional staining.

RT-qPCR detection. Synovial tissue total RNA was extracted using TRNzol (TIANGEN) using standard procedures. The quality of RNA was assessed by measuring the $D(\lambda)_{260}/D(\lambda)_{280}$ ratio using an Infinite-TECAN-enzyme-labeling-instrument (model: M200PRO). Samples with $D(\lambda)_{260}/D(\lambda)_{280}$ falling within the range of 1.8−2.0 were stored for subsequent use. For cDNA synthesis, 1 μg total RNA was utilized with the Fast-Reverse-Transcription-Master-Mix (BIOTECHINC). Residual DNA was eliminated at 42 °C for 5 min, followed by reverse transcription at 42 °C for 15 min, and subsequent inactivation of reverse transcriptase at 95 °C for 5 min. Then, 1.2 μL cDNA was employed for real-time fluorescence PCR reactions. A 2-step thermal cycle was employed as per the instructions of the SYBR-Green-qPCR-Mix-kit (BIOTECHINC). The reaction conditions included 95 °C for 3 min, followed by 40 cycles of 95 °C for 10 s and 60 °C for 30 s. All specimens were loaded onto a 96-well PCR plate, with each specimen being triplicated. The reactions were conducted using a Roche-LightCycler-Sequence-Detection-System. The primer sequences are listed in Table 1. For quantitative analysis, the comparative Ct approach was employed, with GAPDH serving as the internal reference. The $\triangle Ct$ ($Ct_{target} - Ct_{internal\ reference}$) approach was utilized for relative quantitative analysis, and $2^{-\triangle\triangle Ct}$ was calculated to determine the expression level of the target gene.

Statistical Analysis. Statistical tests were performed with SPSS v19.0. Results are presented as mean ± standard deviation (SD). For pairwise comparisons between two groups with normal distribution, the independent-samples t test was employed. In the case of multiple group comparisons, if the variances were homogeneous and the data followed a normal distribution, either the LSD-t or Dunnett test was utilized. If the data did not follow a normal distribution, a nonparametric t test was employed. For cases where the data were normally distributed but the variances were not homogeneous, either Tamhane's T2 or Dunnett's T3 test was used. A significance level of $p \leq 0.05$ was deemed statistically significant.

RESULTS

Identification of the Main Constituents of TFLA. The chemical compositions of TFLA were identified by UPLC-TQF-MS/MS (Figure 2). In total, 55 constituents including saponins, flavonoids, alkaloids, and organic acids were confirmed or tentatively identified according to the accurate mass measurements, fragmentation behavior, and related literatures. A comprehensive list of all the compounds is provided in Table 2.

Predictions by Network Pharmacology. Using TCMSP databases, 421 potential targets for TFLA were predicted (Figure 3A).

To identify potential targets of gouty arthritis, we searched 4 databases for research articles related to the condition. In total,

https://doi.org/10.1021/acsomega.4c00056
ACS Omega 2024, 9, 34303−34313

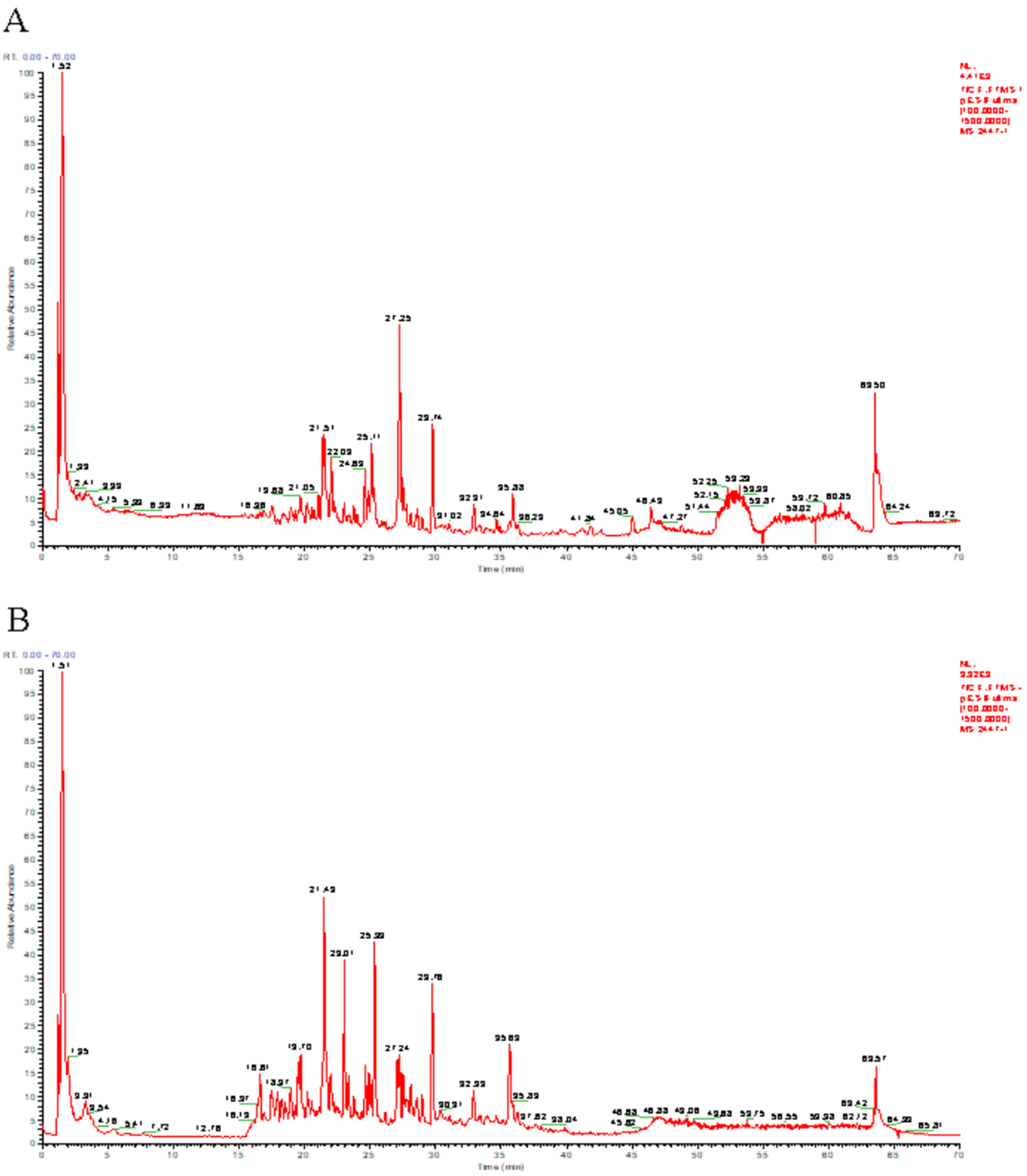

Figure 2. TIC plot in positive and negative ion mode. (A) TIC plot of TFLA in positive ion mode. (B) TIC plot of TFLA in negative ion mode.

we found 1365 targets associated with gouty arthritis, with 1021 from the GeneCards database, and 109, 206, and 29 from the OMIM, DisGeNET, and DrugBank databases, respectively. After eliminating duplicate targets, we identified 1192 targets related to gouty arthritis (Figure 3C).

The subsequent 160 targets of TFLA and GA (Figure 3B) were examined with the STRING database, and a PPI network was built (Figure 4A). Through topological analysis, 20 core targets were obtained based on a card value twice that of the degree, and a corresponding map was generated (Figure 4B).

To explore the crucial biological processes of TFLA in the treatment of gouty arthritis, the GO functional enrichment analyses were performed, which are mainly involved in the positive regulation of chemokine production, positive regulation of gene expression, receptor complex, macromolecular complex,

https://doi.org/10.1021/acsomega.4c00056
ACS Omega 2024, 9, 34303−34313

Table 2. Analysis of the Chemical Constituents of TFLA by UPLC-TOF-MS/MS

no.	RT (min)	measured mass	error (ppm)	molecular formula	identification compound	herb
1	21.799	442.09007	0.17	$C_{22}H_{18}O_{10}$	(−)-epicatechin gallate	HZ
2	22.078	358.14158	−0.15	$C_{20}H_{22}O_6$	(+)-pinoresinol	RDT
3	27.192	162.03157	−0.77	$C_9H_6O_3$	7-hydroxycoumarin	ZJF
4	30.45	368.12588	−0.29	$C_{21}H_{20}O_6$	anhydroicaritin	ZJF
5	27.235	270.05278	−0.17	$C_{15}H_{10}O_5$	apigenin	HZ, CQC, TGC
6	21.696	448.10069	0.29	$C_{21}H_{20}O_{11}$	astragalin	TGC, GC
7	37.093	230.13068	−0.01	$C_{15}H_{18}O_2$	atractylenolide I	ZJF
8	1.508	117.07894	−0.3	$C_5H_{11}NO_2$	betaine	TGC
9	32.775	284.06833	−0.52	$C_{16}H_{12}O_5$	biochanin A	GC
10	23.015	180.0422	−0.34	$C_9H_8O_4$	caffeic acid	CQC
11	34.302	284.06822	−0.88	$C_{16}H_{12}O_5$	calycosin	GC
12	1.584	146.02162	−1.43	$C_6H_8O_7$	citric acid	HZ
13	21.148	164.0473	−0.27	$C_9H_8O_3$	*p*-coumaric acid	ZJF
14	21.238	448.10069	0.29	$C_{21}H_{20}O_{11}$	cynaroside	HZ, CQC
15	24.357	254.05776	−0.59	$C_{15}H_{10}O_4$	daidzein	GC
16	21.091	416.11062	−0.26	$C_{21}H_{20}O_9$	daidzin	GC
17	36.24	414.31319	−0.5	$C_{27}H_{42}O_3$	diosgenin	FBX
18	35.647	270.05277	−0.21	$C_{15}H_{10}O_5$	emodin	HZ
19	22.929	262.08559	0.42	$C_{16}H_{12}O_5$	emodin-3-methyl ether/physcion	HZ
20	19.425	178.0266	−0.03	$C_9H_6O_4$	esculetin	TGC
21	22.918	286.04751	−0.81	$C_{15}H_{10}O_6$	fisetin	GC
22	29.308	268.07351	−0.19	$C_{16}H_{12}O_4$	formononetin	GC
23	7.696	170.02151	−0.08	$C_7H_6O_5$	gallic acid	HZ
24	22.804	270.05259	−0.88	$C_{15}H_{10}O_5$	genistein	HZ
25	27.063	284.0683	−0.6	$C_{16}H_{12}O_5$	glycitein	GC
26	21.675	464.09576	0.6	$C_{21}H_{20}O_{12}$	hyperoside	HZ, RDT
27	21.951	624.20561	0.3	$C_{29}H_{36}O_{15}$	isoacteoside	CQC
28	22.026	222.05262	−0.92	$C_{11}H_{10}O_5$	isofraxidin	ZJF
29	21.522	256.07319	−1.43	$C_{15}H_{12}O_4$	isoliquiritigenin	GC
30	20.811	464.09567	0.42	$C_{21}H_{20}O_{12}$	isoquercitrin	HZ, TGC
31	21.768	192.04224	−0.11	$C_{10}H_8O_4$	isoscopoletin	RDT
32	19.422	186.05286	−0.12	$C_8H_8O_4$	isovanillic acid	TGC
33	21.453	864.2109	0.42	$C_{21}H_{20}O_{10}$	isovitexin	GC
34	24.527	286.08403	−0.32	$C_{16}H_{14}O_5$	licochalcone B	GC
35	24.905	256.07341	−0.57	$C_{15}H_{12}O_4$	liquiritigenin	GC
36	17.947	376.1369	−0.12	$C_{16}H_{24}O_{10}$	loganic acid	RDT
37	25.394	286.04762	−0.41	$C_{15}H_{10}O_6$	luteolin	HZ, CQC
38	21.277	302.04234	−1.02	$C_{15}H_{10}O_7$	morin	HZ
39	42.537	422.17278	−0.38	$C_{25}H_{26}O_6$	mulberrin	HZ
40	23.74	430.12618	−0.48	$C_{22}H_{22}O_9$	ononin	GC
41	21.464	390.13134	−0.32	$C_{20}H_{22}O_8$	polydatin	HZ
42	17.834	138.03161	−0.64	$C_7H_6O_3$	protocatechualdehyde	HZ
43	16.025	154.02658	−0.19	$C_7H_6O_4$	protocatechuic acid	ZJF, HZ, TGC, GC
44	26.099	284.06822	−0.88	$C_{16}H_{12}O_5$	prunetin	GC
45	1.486	504.1692	0.33	$C_{18}H_{32}O_{16}$	raffinose	CQC
46	21.465	228.07851	−0.6	$C_{14}H_{12}O_3$	resveratrol	HZ
47	19.865	360.08464	0.34	$C_{18}H_{16}O_8$	rosmarinic acid	ZJF
48	21.276	610.15334	−0.07	$C_{27}H_{30}O_{16}$	rutin	ZJF, TGC, GC
49	15.957	138.0316	−0.69	$C_7H_6O_3$	salicylic acid	CQC
50	24.566	494.12129	−0.01	$C_{26}H_{22}O_{10}$	salvianolic acid A	XCQ
51	20.296	282.07396	0.27	$C_{26}H_{28}O_{14}$	schaftoside	CQC
52	21.724	286.04745	−1.01	$C_{15}H_{10}O_6$	scutellarein	CQC
53	2.258	174.05264	−1.05	$C_7H_{10}O_5$	shikimic acid	RDT
54	1.533	161.10517	0.3	$C_7H_{13}NO_2$	stachydrine	TGC
55	1.522	155.05823	−1.02	$C_7H_7NO_2$	trigonelline HCl	RDT

NAD^+ nucleosidase activity, cytokine activity, and other biological processes (Figure 5A).

KEGG pathway analysis was conducted on these core targets, and the top 20 pathways, ranked by *p*-value, were utilized to establish an advanced plot chart (Figure 5B). According to KEGG data, Inflammatory Bowel Disease as well as signaling pathways of IL17, Toll-like receptor, C-type lectin receptor, and TNF were closely associated with gouty arthritis.

https://doi.org/10.1021/acsomega.4c00056
ACS Omega 2024, 9, 34303−34313

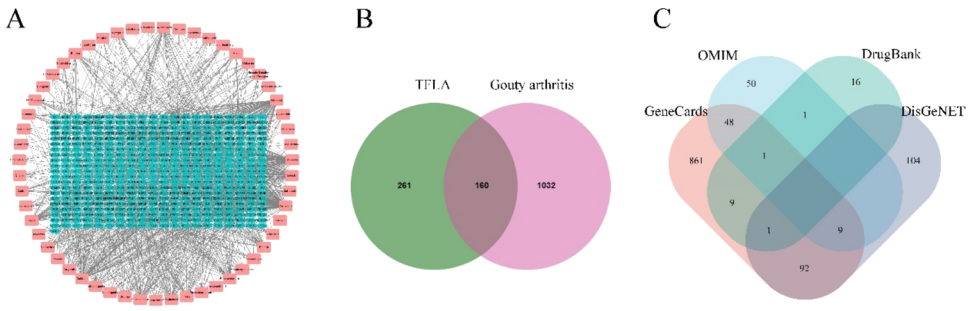

Figure 3. Drug-target-disease network and PPI network construction. (A) The network of drug-target diseases includes 7 kinds of herbs, 55 active components, and 421 target genes. (B) The intersection targets of gouty arthritis-related targets and TFLA-related targets. (C) The collection of predictive targets for gouty arthritis.

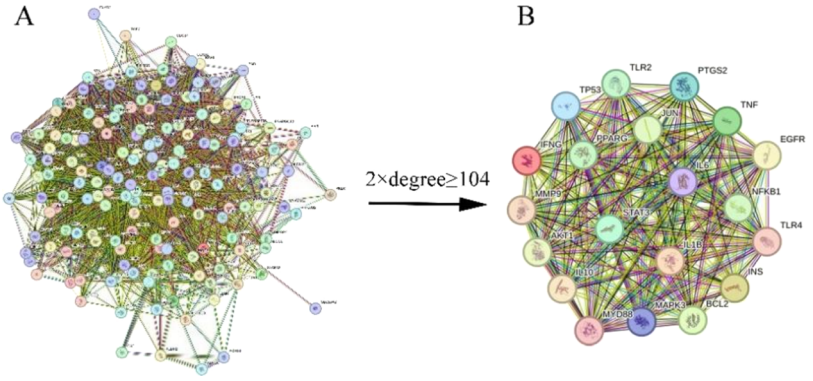

Figure 4. Protein−protein Interaction Network. (A) PPI network of predicted targets of TFLA against gouty arthritis. (B) The significant proteins of the PPI network were extracted from the cellular compartment of (A).

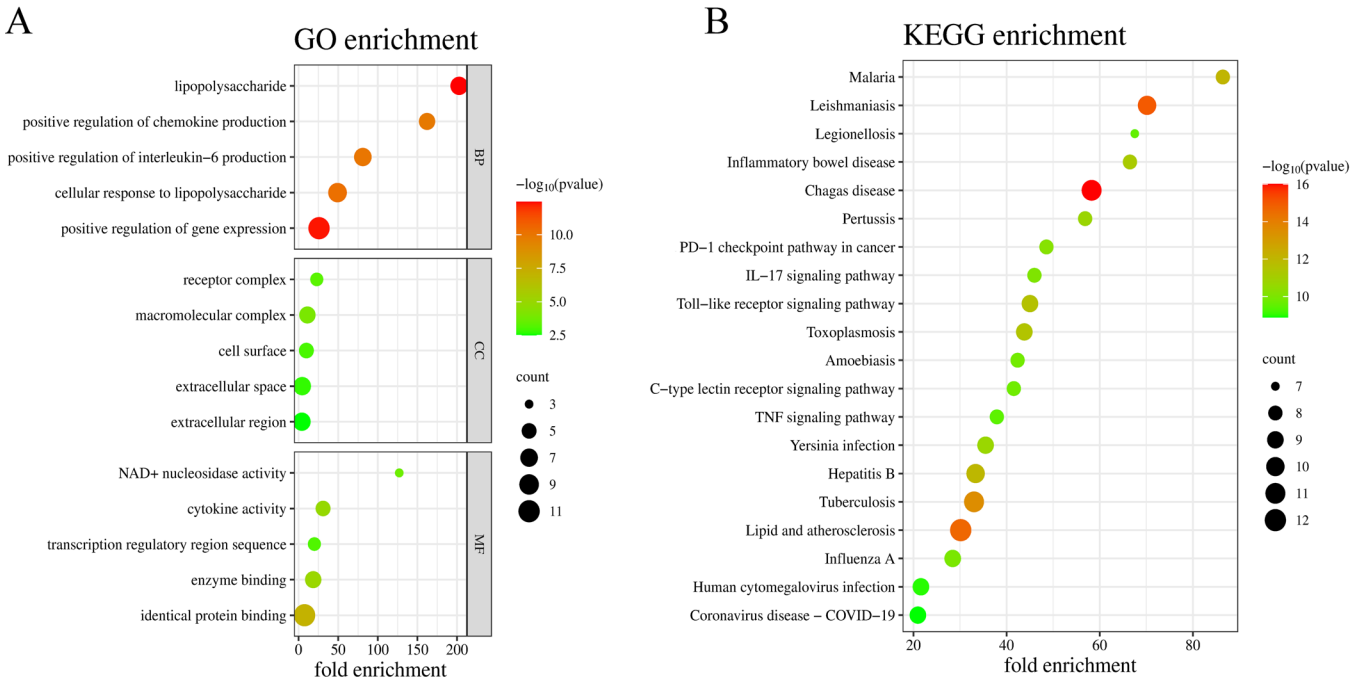

Figure 5. GO and KEGG functional analysis. (A) The top 20 of GO enrichment analysis in Biological processes (BP), cellular components (CC), and molecular function (MF). (B) The top 20 signaling pathways were analyzed by KEGG.

Previous studies from our team have confirmed IL17, VEGFA, NF-κB p65, and IL1β as potential targets of TFLA for antigout effects. Hence, this paper focuses on investigating whether TFLA exerts an anti-gouty arthritis role by impacting the Toll-like receptor signaling pathway.

TFLA Relieves the Swelling of the Ankle Joint. Six hours after injection of MSU crystals, the rats' ankle joint showed obvious redness, swelling, and deformity (Figure 6). Subsequently, the perimeter of the rats' ankle joints was measured at various time points to quantify the degree of joint swelling.

https://doi.org/10.1021/acsomega.4c00056
ACS Omega 2024, 9, 34303−34313

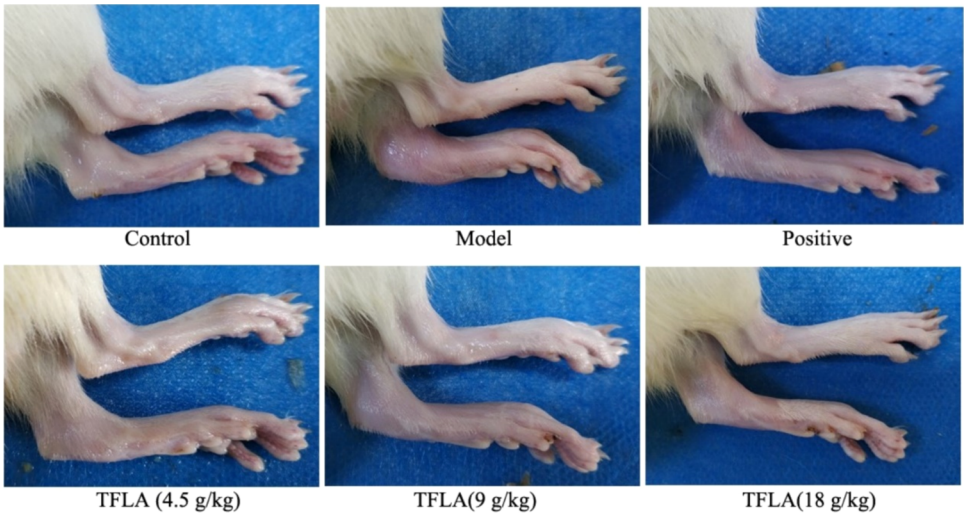

Figure 6. MSU crystals induced gouty arthritis in rats. The swelling of the joint was clearly observed 12 h after the MSU injection.

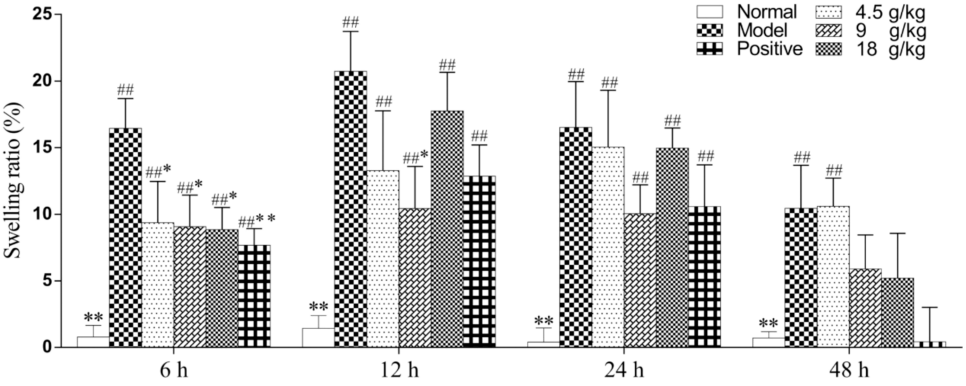

Figure 7. Effects of TFLA on the swelling rate of ankle joint in MSU crystals-injected rats. Measurement data represent the mean ± SD (n = 10). One-way ANOVA and Dunnett test were used for statistical analysis. $^{\#}p \leq 0.05$, $^{\#\#}p \leq 0.01$ as compared to the Normal group. $^{*}p \leq 0.05$, $^{**}p \leq 0.01$ as compared to the Model group.

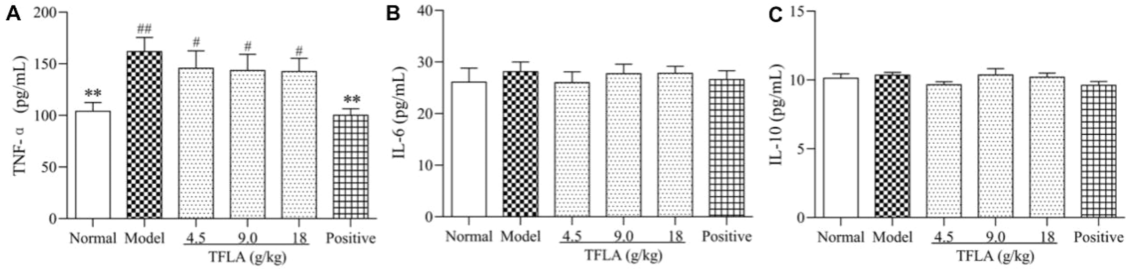

Figure 8. Effects of TFLA on serum inflammatory cytokines in rats: (A) TNF-α content. (B) IL6 content. (C) IL10 content. Measurement data represent the mean ± SD (n = 10). One-way ANOVA and Dunnett test were used for statistical analysis. $^{\#}p \leq 0.05$, $^{\#\#}p \leq 0.01$ as compared to the Normal group. $^{*}p \leq 0.05$, $^{**}p \leq 0.01$ as compared to the Model group.

Comparative analysis revealed a significant increase in swelling of the left ankle joint in rats following MSU injection, with percentages of 16.5, 20.7, 16.5, and 10.5% at 6, 12, 24, and 48 h, respectively (as depicted in Figure 7), compared to the control group. These findings imply that TFLA treatments exert varying degrees of inhibitory effects on ankle swelling. Notably, TFLA exhibited promising inhibitory effects during the initial stages of MSU injection.

TFLA Decreases the Levels of Inflammatory Cytokines. Prior research has established a correlation between gout's pathogenesis and inflammation, with acute gouty arthritis distinguished by elevated expression of inflammatory cytokines.[24−26] In this investigation, the ELISA method was employed to measure the serum levels of inflammatory cytokines. As depicted in Figure 8, the levels of TNFα, IL6, and IL10 in the TFLA treatment group were remarkably lower compared with the model group.

TFLA Improves Histopathological Changes of Ankle Joint Synovium. In the model group, obvious pathological alterations, such as synovial hyperplasia, edema, vascular hyperemia, capillary hyperplasia, and elevated inflammatory cell infiltration, were evident in the synovium of the ankle joint.

https://doi.org/10.1021/acsomega.4c00056
ACS Omega 2024, 9, 34303−34313

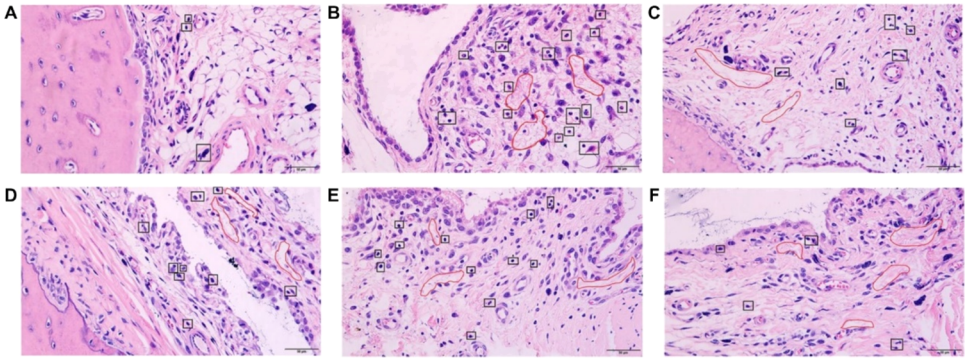

Figure 9. Effect of TFLA on pathological changes of joint synovial tissue. (A) Normal group (injection of PBS). (B) Model group (with injection of MSU crystals). (C) Allopurinol + Colchicine group. (D) TFLA (4.5 g/kg) group. (E) TFLA (9 g/kg) group. (F) TFLA (18 g/kg) group. The red box indicates the site of synovial edema, and the black box indicates the site of inflammatory cell infiltration.

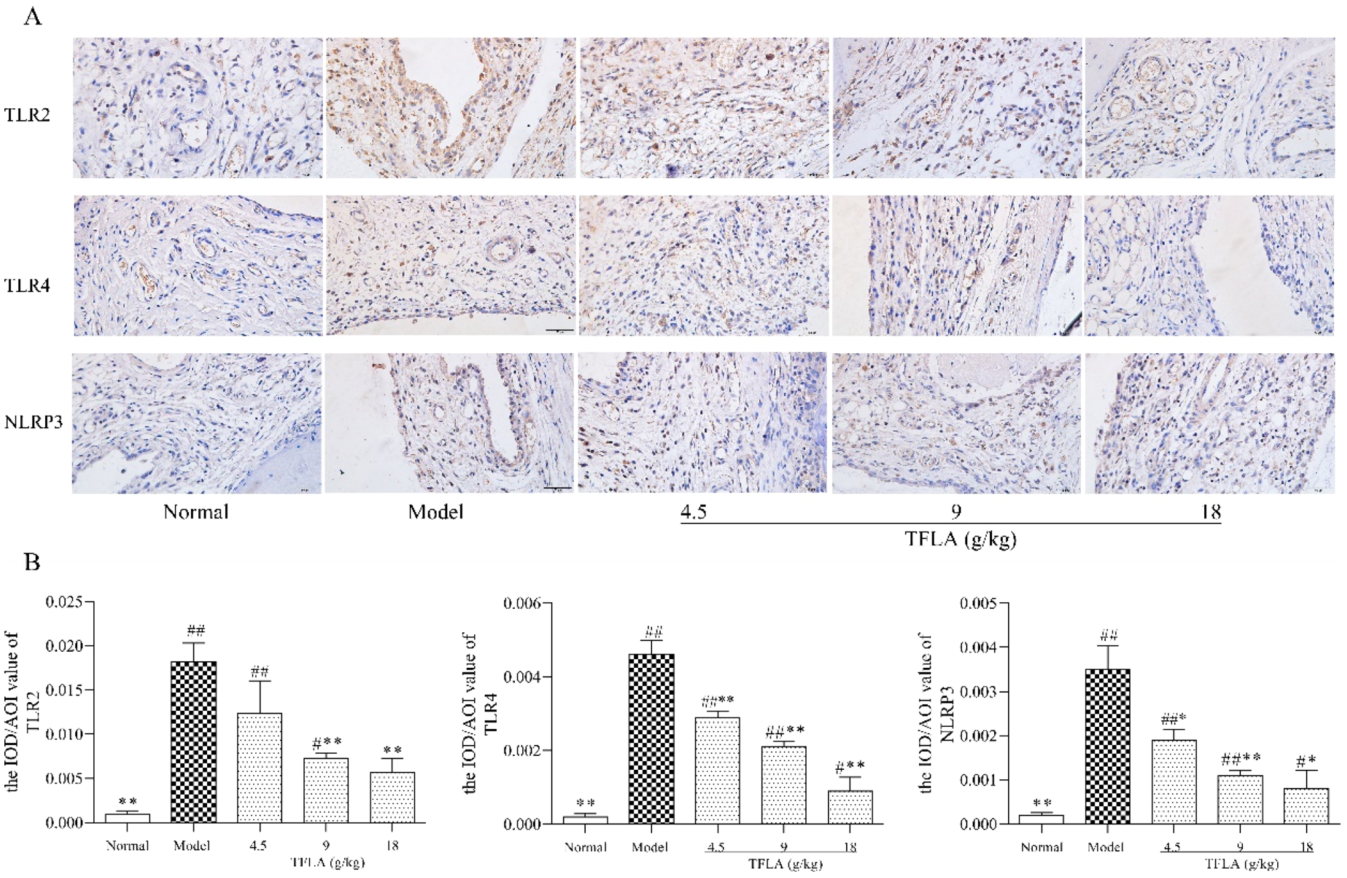

Figure 10. Effect of TFLA on the protein expression of TLR2 and TLR4 in synovial tissue. (A) Representation of synovial tissue in five groups by using semiquantitative immunohistochemistry (magnification ×400). (B) Statistical analysis of data on the expression of TLR2 and TLR4 in synovial tissue. Measurement data represent the mean ± SD ($n = 10$). One-way ANOVA followed by the Dunnett test was used for statistical analysis. $^{\#}p \leq 0.05$, $^{\#\#}p \leq 0.01$ as compared to the Normal group. $^{*}p \leq 0.05$, $^{**}p \leq 0.01$ as compared to the Model group.

However, TFLA treatment ameliorated synovial hyperplasia and diminished the infiltration of inflammatory cells into the synovium (Figure 9). These findings indicate that TFLA holds potential in mitigating joint injury.

TFLA Reduces the Protein Expression of TLR2, TLR4, and NLRP3 in the Synovium. As illustrated in Figure 10, the IOD/AOI values of TLR2, TLR4, and NLRP3 positive staining areas in the ankle synovium of the model group exhibited a significant increase compared with the normal group ($p < 0.01$). Conversely, in comparison to the model group, all doses of TFLA notably reduced the IOD/AOI values of TLR2, TLR4, and NLRP3. Notably, the IOD/AOI values of TLR2 and TLR4 expression displayed dose-dependent trends. From these observations, we infers that TFLA exerts an anti-inflammatory effect by modulating the TLR pathway and NLRP3.

TFLA Downregulates TLR2, TLR4, and NF-κB Gene Expression in Synovium. In comparison to those in the normal group, the expression levels of TLR2, TLR4, and NFκB were markedly elevated in the model group. Conversely, in the TFLA group, the expression levels of TLR2, TLR4, and NFκB were remarkably lower than those observed in the model group. Notably, the reduction in TLR2 and NFκB mRNA levels

https://doi.org/10.1021/acsomega.4c00056
ACS Omega 2024, 9, 34303−34313

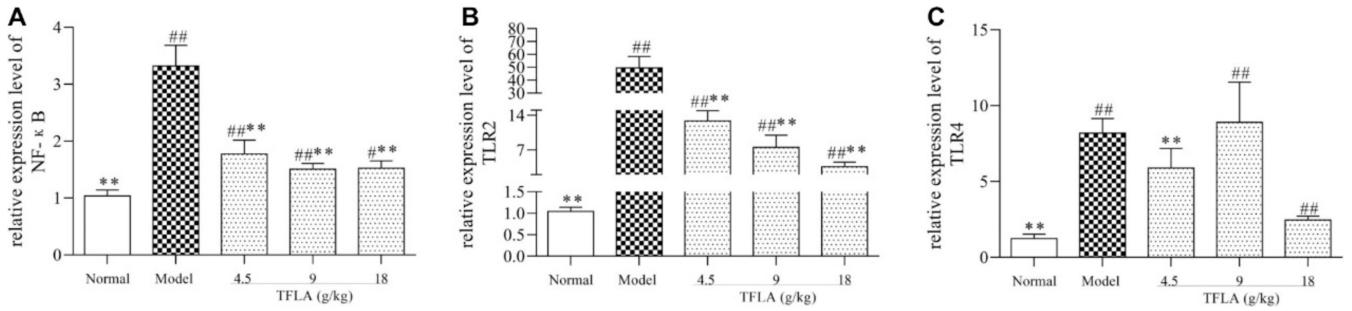

Figure 11. Effects of several gene expressions in synovial tissue. (A). Relative expression level of NF-κB. (B) Relative expression level of TLR2. (C) Relative expression level of TLR4. and Measurement data represent the mean ± SD ($n = 10$). One-way ANOVA followed by the Dunnett test was used for statistical analysis. $^{\#}p \leq 0.05$, $^{\#\#}p \leq 0.01$ as compared to the Normal group. $^{*}p \leq 0.05$, $^{**}p \leq 0.01$ as compared to the Model group.

exhibited a dose-dependent relationship (Figure 11). These findings provide further confirmation that the anti-inflammatory properties of TFLA are closely associated with the TLR/NFκB pathway.

DISCUSSION

Existing evidence has demonstrated that traditional medicine could be used with low toxicity in treating gouty arthritis.[27] Herein, we evaluated the effects and molecular mechanisms of TFLA, a new traditional medicine granule, in an MSU-induced gouty arthritis rat model. The chemical components of TFLA include saponins, flavonoids, alkaloids, and organic acids. Utilizing UPLC-Q-TOF/MS, we identified 55 compounds such as Apigenin, Astragalin, Hyperoside, and Protocatechuic acid, shedding light on the primary chemical constituents of TFLA. Network pharmacology, a systematic and holistic medical research paradigm, is known for systematically uncovering the biological basis of Traditional Chinese Medicines (TCMs). It has been extensively employed in researching the bioactive ingredients, syndromes, formulas, and other aspects of TCMs.[28] Numerous scholars have conducted comprehensive studies on the complex system of TCMs, leveraging network pharmacological methodologies from various perspectives. Their investigations have yielded significant findings and insights crucial for confirming the presence of and elucidating the mechanisms of bioactive substances inherent in TCMs. This study conducted network pharmacology analysis based on compounds identified by UPLC-Q-TOF/MS. The "drug-ingredient-target-disease" network revealed that multiple compounds in TFLA could act on multiple targets related to gouty arthritis. GO enrichment analysis also indicated that the positive regulation of chemokine production, positive regulation of gene expression, receptor complex formation, macromolecular complex formation, cytokine activity, and other biological processes play essential roles, indicating potential anti-inflammatory and analgesic effects. Additionally, through KEGG pathway analysis, we focused on the TLRs signaling pathway, which exhibited the most significant p-value. Hence, TFLA may regulate targets associated with gouty arthritis through the TLRs pathway.

Acute gouty arthritis manifests as an intense inflammatory response triggered by the deposition of MSU crystals.[29,30] During an acute attack, these crystals promote the secretion of cytokines such as IL1β, IL6, and TNFα, inducing the infiltration of inflammatory cells, such as neutrophils and monocytes, into the joint synovium. This process increases vascular permeability, leading to symptoms such as redness, swelling, and pain.[31] The onset of acute gouty arthritis typically occurs 12−24 h after the initial attack, with inflammation peaking and usually subsiding within 1−2 weeks.[32] Animal models of MSU-induced gouty arthritis provide valuable insights into the mechanisms of inflammation. In this study, we monitored the inflammatory response in the ankle joints of rats following the MSU injection. The degree of joint swelling was the most obvious at 12 h after MSU administration. Pathological analysis revealed synovial hyperplasia, inflammatory cell infiltration, and vascular dilatation in the right posterior ankle joint of rats exposed to MSU crystals. Treatment with TFLA obviously reduced ankle joint swelling and mitigated the inflammatory reaction compared to the model group.

The body's immune system identifies MSU crystals as foreign invaders, triggering the innate immune response and leading to inflammation through signal transmission.[33,34] These crystals, which are endogenous danger signals, are detected by pattern-recognition receptors (PRRs), including both intracellular receptors (NLRs) and membrane receptors (TLRs). Recognition of MSU crystals can activate TLRs and the NALP3 inflammasome signal transduction, which controls the secretion of IL1β. The TLR and NLR pathways play critical roles in the development of acute gouty arthritis.[29] TLR serves as a key PRR in innate immunity, and its signaling pathway is crucial in inflammation.[35,36] TLR2 and TLR4 signal transmission can engage MyD88 via specific ligands, thereby activating downstream transcription factors such as NFκB, which initiates the expression of IL1β, IL6, IL8, and TNFα.[37,38] Our findings indicated an obvious increase in the levels of TLR2, TLR4 mRNA, and protein in the synovial tissues of rats with MSU-induced arthritis. Moreover, activated NFκB mRNA and protein levels were notably elevated, further promoting the expression of inflammatory cytokines and triggering an inflammatory cascade. Treatment with TFLA significantly decreased the levels of TLR2, TLR4, and NFκB mRNA and protein, indicating that TFLA can downregulate the TLR/NFκB axis and inhibit the expression of downstream inflammatory cytokines.

Research has demonstrated that NLRP3 inflammatory bodies play a vital role in sensing MSU crystal deposits and subsequently activating downstream innate immune responses.[39−41] MSU crystals activate NLRP3 inflammatory bodies, leading to the production of active IL1β and IL8.[42,43] Our immunohistochemical findings demonstrated that NLRP3 expression was remarkably higher in the model group than in the normal group, and treatment with TFLA could inhibit the activation of NLRP3 inflammasomes, thereby exerting an anti-inflammatory effect.

https://doi.org/10.1021/acsomega.4c00056
ACS Omega 2024, 9, 34303−34313

CONCLUSIONS

In summary, our research suggests that TFLA exhibits a robust protective effect against MSU-induced acute gouty arthritis in rats. This effect is likely achieved through the reduction of joint tissue damage, lowering inflammatory cytokine levels in the bloodstream and downregulating the TLRs/NFκB/NLRP3 inflammatory axis. This study provides a scientific foundation for the further development of traditional medicine preparations in this field. However, the multifaceted mechanism of action of TFLA in acute gouty arthritis requires further investigation in future studies.

AUTHOR INFORMATION

Corresponding Authors

Fengzhen Li − *International Zhuang Medicine Hospital Affiliated to Guangxi University of Chinese Medicine, Nanning 530201 Guangxi, China*; Email: lifengzhen2005@163.com

Zongxi Sun − *International Zhuang Medicine Hospital Affiliated to Guangxi University of Chinese Medicine, Nanning 530201 Guangxi, China*; Email: sunzx@gxtcmu.edu.cn

Authors

Xiangpei Zhao − *International Zhuang Medicine Hospital Affiliated to Guangxi University of Chinese Medicine, Nanning 530201 Guangxi, China*; orcid.org/0000-0002-2823-5392

Zhaoyang Long − *International Zhuang Medicine Hospital Affiliated to Guangxi University of Chinese Medicine, Nanning 530201 Guangxi, China*

Hua Zhong − *International Zhuang Medicine Hospital Affiliated to Guangxi University of Chinese Medicine, Nanning 530201 Guangxi, China*

Rongping Lu − *International Zhuang Medicine Hospital Affiliated to Guangxi University of Chinese Medicine, Nanning 530201 Guangxi, China*

Juan Wei − *International Zhuang Medicine Hospital Affiliated to Guangxi University of Chinese Medicine, Nanning 530201 Guangxi, China*

Complete contact information is available at: https://pubs.acs.org/10.1021/acsomega.4c00056

Author Contributions

†F.L. and Z.S. contributed equally to this work. X.Z., Z.L., and H.Z. carried out the studies, participated in collecting data, and drafted the manuscript. Z.S. and F.L. performed the statistical analysis and participated in its design. R.L. was responsible for revising the manuscript. All authors read and approved the final manuscript.

Funding

This work was supported by National Natural Science Foundation of China (NSFC) [No. 82260980]; Doctor Start-up Fund from the Guangxi University of Chinese Medicine [No. 2019BS044]; Three-year Action Plan Project for the Construction of High-level Talent Team of International Zhuang Medicine Hospital Affiliated to Guangxi University of Chinese Medicine (GZCX20231204).

Notes

The authors declare no competing financial interest.

The authors are accountable for all aspects of the work in ensuring that questions related to the accuracy or integrity of any part of the work are appropriately investigated and resolved. The trial was conducted in accordance with the Declaration of Helsinki (as revised in 2013). The study was approved by the Ethics Committee of Guangxi International Zhuang Medicine Hospital (Ethics No. DW2020618-31).

REFERENCES

(1) Chi, X.; Zhang, H.; Zhang, S.; Ma, K. Chinese herbal medicine for gout: a review of the clinical evidence and pharmacological mechanisms. *Chin. Med.* **2020**, *15*, 17.

(2) Wang, H.; Duan, H.; Chen, S.; Luo, Y.; Zhang, Y.; Liu, Q.; Zhang, X. Chinese herbal medicine si-miao-san decoction for acute gouty arthritis: A protocol for systematic review and meta-analysis of randomized controlled trials. *Medicine* **2020**, *99* (32), No. e21510.

(3) Lyu, S.; Ding, R.; Liu, P.; Ouyang, H.; Feng, Y.; Rao, Y.; Yang, S. LC-MS Analysis of Serum for the Metabolomic Investigation of the Effects of Pulchinenoside b4 Administration in Monosodium Urate Crystal-Induced Gouty Arthritis Rat Model. *Molecules* **2019**, *24* (17), No. 3161, DOI: 10.3390/molecules24173161.

(4) Towiwat, P.; Chhana, A.; Dalbeth, N. The anatomical pathology of gout: a systematic literature review. *BMC Musculoskelet. Disord.* **2019**, *20* (1), 140.

(5) Bardin, T.; Richette, P. Impact of comorbidities on gout and hyperuricaemia: an update on prevalence and treatment options. *BMC Med.* **2017**, *15* (1), 123.

(6) Li, Z.; Zhou, Z.; Hou, X.; Lu, D.; Yuan, X.; Lu, J.; Wang, C.; Han, L.; Cui, L.; Liu, Z.; Chen, J.; Cheng, X.; Zhang, K.; Ji, J.; Jia, Z.; Ma, L.; Xin, Y.; Liu, T.; Yu, Q.; Ren, W.; Wang, X.; Li, X.; Mi, Q.; Shi, Y.; Li, C. Replication of Gout/Urate Concentrations GWAS Susceptibility Loci Associated with Gout in a Han Chinese Population. *Sci. Rep.* **2017**, *7* (1), No. 4094.

(7) Gao, L.; Jiang, Y.; Wang, Y.; Qu, X.; Li, L.; Lou, X.; Wang, Y.; Guo, H.; Liu, Y. Male asymptomatic hyperuricemia patients display a lower number of NKG2D+ NK cells before and after a low-purine diet. *Medicine* **2018**, *97* (50), No. e13668.

(8) Moulay Berkchi, J.; Rkain, H.; Benbrahim, L.; Aktaou, S.; Lazrak, N.; Faiz, S.; Ahid, S.; Abouqal, R.; Labzizi, S.; Ouzeddoun, N.; Oukerraj, L.; Hmamouchi, I.; Hajjaj-Hassouni, N.; Allali, F. Management of gout by Moroccan rheumatologists: a Moroccan Society for Rheumatology National Survey. *Rheumatol. Int.* **2020**, *40* (9), 1399−1408.

(9) Dalbeth, N.; Gosling, A. L.; Gaffo, A.; Abhishek, A. Gout. *Lancet* **2021**, *397* (10287), 1843−1855.

(10) Steinmetz, R. G.; Maxted, M.; Rowles, D. Arthroscopic Management of Intra-articular Tophaceous Gout of the Knee: A Case Report and Review of the Literature. *J. Orthop. Case Rep.* **2018**, *8* (2), 86−89.

(11) Yi, T.; Zhao, Z.; Yu, Z.; Chen, H. Comparison of the anti-inflammatory and anti-nociceptive effects of three medicinal plants known as ″Snow Lotus″ herb in traditional Uighur and Tibetan medicines. *J. Ethnopharmacol.* **2010**, *128* (2), 405−411.

(12) Yang, T.; Yan, D.; Huang, X.; Hou, B.; Ma, Y.; Peng, H.; Zhang, X.; Chen, J.; Geng, C. chalcone-flavonone heterodimers from Terminthia paniculata, and their protective effects on hyperuricemia and acute gouty arthritis. *Phytochemistry* **2019**, *164*, 228−235.

(13) Yi, T.; Lo, H.; Zhao, Z.; Yu, Z.; Yang, Z.; Chen, H. Comparison of the chemical composition and pharmacological effects of the aqueous and ethanolic extracts from a Tibetan ″Snow Lotus″ (Saussurea laniceps) herb. *Molecules* **2012**, *17* (6), 7183−7194.

(14) You, W.; Wang, J.; Zou, Y.; Che, K.; Hou, X.; Fei, H.; Wang, Y. Modified Chuanhu anti-gout mixture, a traditional Chinese medicine, protects against potassium oxonate-induced hyperuricemia and renal dysfunction in mice. *J. Int. Med. Res.* **2019**, *47* (5), 1927−1935.

(15) Zhang, X.-y.; Cheng, J.; Zhao, P.; Chen, K.; Li, J. Screening the Best Compatibility of Selaginella moellendorffii Prescription on Hyperuricemia and Gouty Arthritis and Its Mechanism. *Evid.-Based Complement. Altern. Med.* **2019**, *2019*, No. 7263034.

(16) Yu, D.; Wang, Y.; Yu, C.; Song, M.; Zhou, Q.; Liu, S. High-Throughput Serum Metabolomics Analysis of Gouty Arthritis Rat Treated by Total Saponins of Rhizoma Dioscoreae Makino by UPLC-Q/TOF-MS. *Biomed. Chromatogr.* **2020**, *34* (9), No. e4867.

(17) Chen, J.; Li, T.; Huang, D.; Gong, W.; Tian, J.; Gao, X.; Qin, X.; Du, G.; Zhou, Y. Integrating UHPLC-MS/MS quantitative analysis and exogenous purine supplementation to elucidate the antidepressant mechanism of Chaigui granules by regulating purine metabolism. *J. Pharm. Anal.* **2023**, *13* (12), 1562−1576.
(18) Zhang, X.; Gao, R.; Zhou, Z.; Sun, J.; Tang, X.; Li, J.; Zhou, X.; Shen, T. Uncovering the mechanism of Huanglian-Wuzhuyu herb pair in treating nonalcoholic steatohepatitis based on network pharmacology and experimental validation. *J. Ethnopharmacol.* **2022**, *296*, No. 115405.
(19) Lee, Y. M.; Shon, E.; Kim, O.; Kim, D. Effects of Mollugo pentaphylla extract on monosodium urate crystal-induced gouty arthritis in mice. *BMC Complement. Altern. Med.* **2017**, *17* (1), 447.
(20) Zhang, K.-h.; Wang, M.; Wei, L.; Feng, C.; Zhang, Y.; Teng, J. Investigation of the Effects and Mechanisms of Dendrobium loddigesii Rolfe Extract on the Treatment of Gout. *Evid.-Based Complement. Altern. Med.* **2020**, *2020*, No. 4367347.
(21) Chen, G.; Jia, P.; Yin, Z.; Kong, S.; Xiang, Z.; Zheng, X. Paeonol ameliorates monosodium urate-induced arthritis in rats through inhibiting nuclear factor-kappaB-mediated proinflammatory cytokine production. *Phytother. Res.* **2019**, *33* (11), 2971−2978.
(22) Li, L.; Wang, D.; Wang, X.; Bai, R.; Wang, C.; Gao, Y.; Anastassiades, T. N-Butyrylated hyaluronic acid ameliorates gout and hyperuricemia in animal models. *Pharm. Biol.* **2019**, *57* (1), 717−728.
(23) Lu, X.; Zeng, R.; Lin, J.; Hu, J.; Rong, Z.; Xu, W.; Liu, Z.; Zeng, W. Pharmacological basis for use of madecassoside in gouty arthritis: anti-inflammatory, anti-hyperuricemic, and NLRP3 inhibition. *Immunopharmacol. Immunotoxicol.* **2019**, *41* (2), 277−284.
(24) Horváthová, V.; Bohatá, J.; Pavlíková, M.; Pavelcová, K.; Pavelka, K.; Šenolt, L.; Stibůrková, B. Interaction of the p.Q141K Variant of the ABCG2 Gene with Clinical Data and Cytokine Levels in Primary Hyperuricemia and Gout. *J. Clin. Med.* **2019**, *8* (11), No. 1965, DOI: 10.3390/jcm8111965.
(25) Lodhi, S.; Vadnere, G.; Patil, K.; Patil, T. Protective effects of luteolin on injury induced inflammation through reduction of tissue uric acid and pro-inflammatory cytokines in rats. *J. Tradit. Complement. Med.* **2020**, *10* (1), 60−69.
(26) Liu, Y.-F.; Xing, G.; Chen, Z.; Tu, S. Long non-coding RNA HOTAIR knockdown alleviates gouty arthritis through miR-20b upregulation and NLRP3 downregulation. *Cell Cycle* **2021**, *20* (3), 332−344.
(27) Liu, P.; Xu, Y.; Ye, J.; Tan, J.; Hou, J.; Wang, Y.; Li, J.; Cui, W.; Wang, S.; Zhao, Q. Qingre Huazhuo Jiangsuan Decoction promotes autophagy by inhibiting PI3K/AKT/mTOR signaling pathway to relieve acute gouty arthritis. *J. Ethnopharmacol.* **2023**, *302* (Pt A), No. 115875.
(28) Wang, Z.; Li, S. Network pharmacology in quality control of traditional Chinese medicines. *Chin. Herb. Med.* **2022**, *14* (4), 477−478.
(29) Tao, J.; Cheng, M.; Tang, J.; Dai, X.; Zhang, Y.; Li, X.; Liu, Q.; Wang, Y. Single nucleotide polymorphisms associated with P2 × 7R function regulate the onset of gouty arthritis. *PLoS One* **2017**, *12* (8), No. e0181685.
(30) Rahmi, E. P.; Kumolosasi, E.; Jalil, J.; Husain, K.; Buang, F.; Abd Razak, A.; Jamal, J. Anti-hyperuricemic and Anti-inflammatory Effects of Marantodes pumilum as Potential Treatment for Gout. *Front. Pharmacol.* **2020**, *11*, 289.
(31) Keller, S. F.; Mandell, B. Management and Cure of Gouty Arthritis. *Med. Clin. North Am.* **2021**, *105* (2), 297−310.
(32) Li, R.; Zhang, P.; Hu, Z.; Yi, Y.; Chen, L.; Zhang, H.; Li, H.; Liu, W.; Wu, M. Efficacy and safety of pricking-blood therapy for acute gouty arthritis: A protocol for systematic review and meta-analysis. *Medicine* **2020**, *99* (50), No. e23521.
(33) Pecherstorfer, C.; Simon, D.; Unbehend, S.; Ellmann, H.; Englbrecht, M.; Hartmann, F.; Figueiredo, C.; Hueber, A.; Haschka, J.; Kocijan, R.; Kleyer, A.; Schett, G.; Rech, J.; Bayat, S. A Detailed Analysis of the Association between Urate Deposition and Erosions and Osteophytes in Gout. *ACR Open Rheumatol.* **2020**, *2* (10), 565−572.
(34) Wang, Y.; Wu, Y.; Xing, Q.; Chu, N.; Shen, L.; Yu, X.; Wang, L. Genetic association of polymorphism rs2230054 in CXCR2 gene with gout in Chinese Han male population. *Cent. Eur. J. Immunol.* **2020**, *45* (1), 80−85.
(35) McCormack, W. J.; Parker, A.; O'Neill, L. Toll-like receptors and NOD-like receptors in rheumatic diseases. *Arthritis Res. Ther.* **2009**, *11* (5), 243.
(36) Cai, Y.; Peng, Y.; Tang, Z.; Guo, X.; Qing, Y.; Liang, S.; Jiang, H.; Dang, W.; Ma, Q.; He, C. Association of Toll-like receptor 2 polymorphisms with gout. *Biomed. Rep.* **2014**, *2* (2), 292−296.
(37) Cabău, G.; Crisan, T.; Kluck, V.; Popp, R.; Joosten, L. Urate-induced immune programming: Consequences for gouty arthritis and hyperuricemia. *Immunol. Rev.* **2020**, *294* (1), 92−105.
(38) Panaro, M. A.; Corrado, A.; Benameur, T.; Paolo, C.; Cici, D.; Porro, C. The Emerging Role of Curcumin in the Modulation of TLR-4 Signaling Pathway: Focus on Neuroprotective and Anti-Rheumatic Properties. *Int. J. Mol. Sci.* **2020**, *21* (7), 2299.
(39) Kingsbury, S.; Conaghan, P.; McDermott, M. The role of the NLRP3 inflammasome in gout. *J. Inflamm. Res.* **2011**, *4*, 39−49.
(40) Yang, C.-S.; Shin, D.; Jo, E. The Role of NLR-related Protein 3 Inflammasome in Host Defense and Inflammatory Diseases. *Int. Neurourol. J.* **2012**, *16* (1), 2−12.
(41) Galvão, I.; Queiroz-Junior, C.; de Oliveira, V.; Pinho, V.; Hirsch, E.; Teixeira, M. The Inhibition of Phosphoinositide-3 Kinases Induce Resolution of Inflammation in a Gout Model. *Front. Pharmacol.* **2019**, *9*, 1505.
(42) Sil, P.; Wicklum, H.; Surell, C.; Rada, B. Macrophage-derived IL-1beta enhances monosodium urate crystal-triggered NET formation. *Inflamm. Res.* **2017**, *66* (3), 227−237.
(43) Lv, H.; Chen, J.; Liu, F.; Jin, Y.; Xu, Z.; Wen, C.; Yu, J. A Traditional Clinic Chinese Medicine Prescription Qu-Zhuo-Tong-Bi (QZTB) Alleviates Gouty Arthritis in Model Rats. *Evid.-Based Complement. Altern. Med.* **2019**, *2019*, No. 9456318.

https://doi.org/10.1021/acsomega.4c00056
ACS Omega 2024, 9, 34303−34313